Electronic Supplementary Material (ESI) for Physical Chemistry Chemical Physics.

Supplementary information:

First-principle calculations of 0D/2D GQDs-MoS_2 mixed van der Waals heterojunctions for photocatalysis: a transition from type I to type II

Li-Long Luo[a], Ping-Xia Wang[a], Xiang-Yan Geng[a], Ying-Tao Liu[a], Roberts I. Eglitis[b], Hong-Qiang Xia[a], Xiao-Yong Lai[a] and Xin Wang[a,*]

[a]State Key Laboratory of High-efficiency Utilization of Coal and Green Chemical Engineering, National Demonstration Center for Experimental Chemistry Education, College of Chemistry and Chemical Engineering, Ningxia University, Yinchuan 750021, China

[b]Institute of Solid State Physics, University of Latvia, 8 Kengaraga Str., Riga LV1067, Latvia

E-mail addresses: wangxin@nxu.edu.cn (X. Wang)

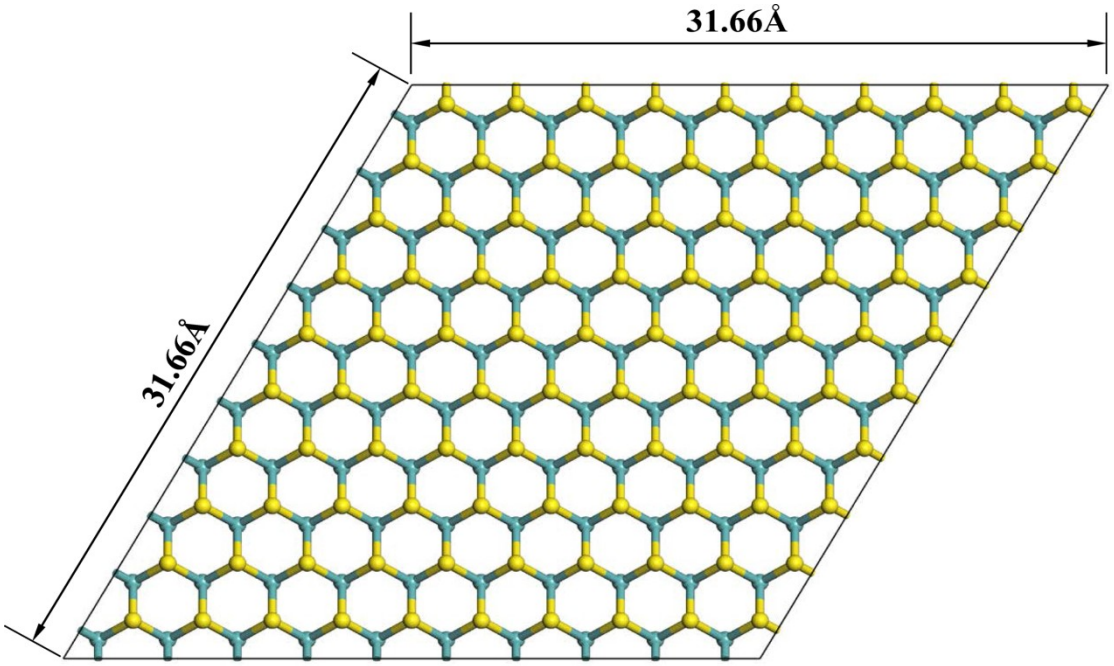

Figure S1 Structure of MoS_2.

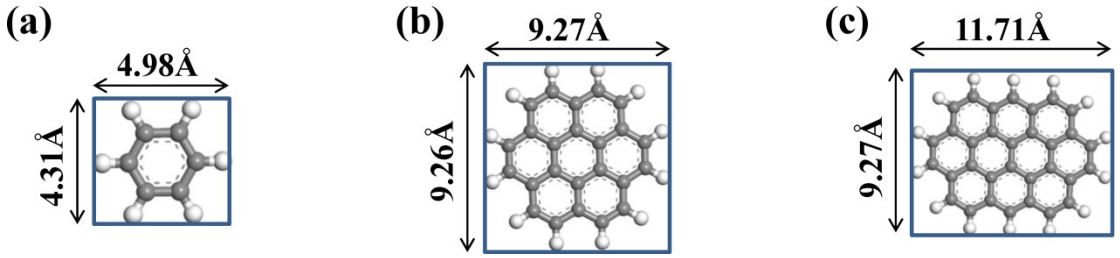

Figure S2 Structures of (a) C_6H_6, (b) $C_{24}H_{12}$, and (c) $C_{32}H_{14}$.

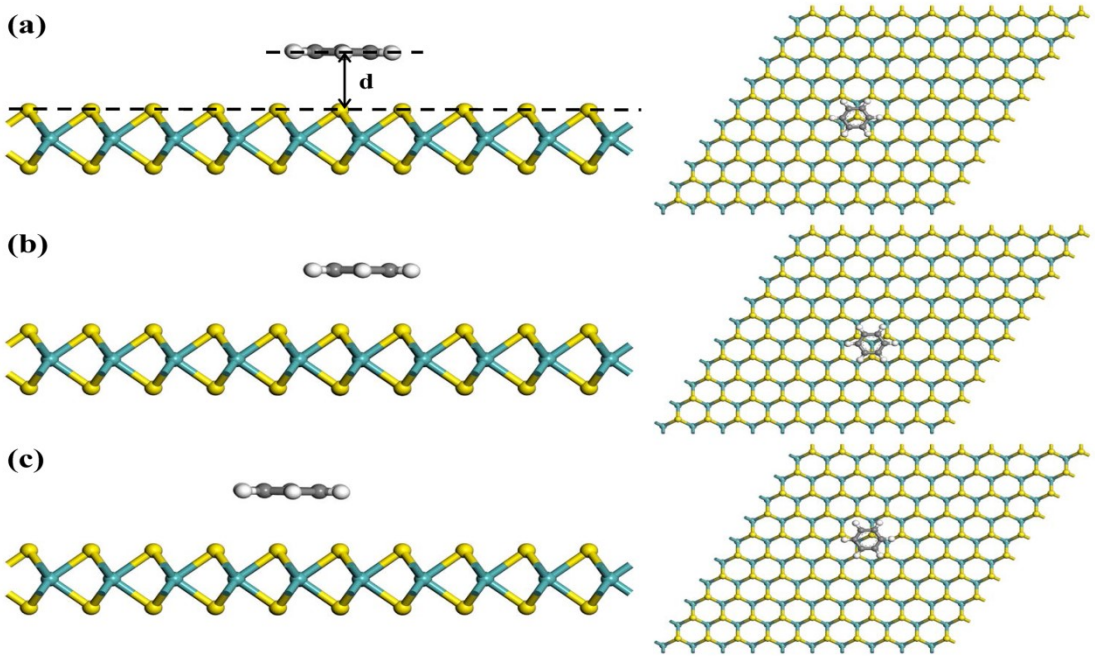

Figure S3 Structures (top view-left and side view-right) of (a) C_6H_6-top, (b) C_6H_6-hollow, and (c) C_6H_6-bridge.

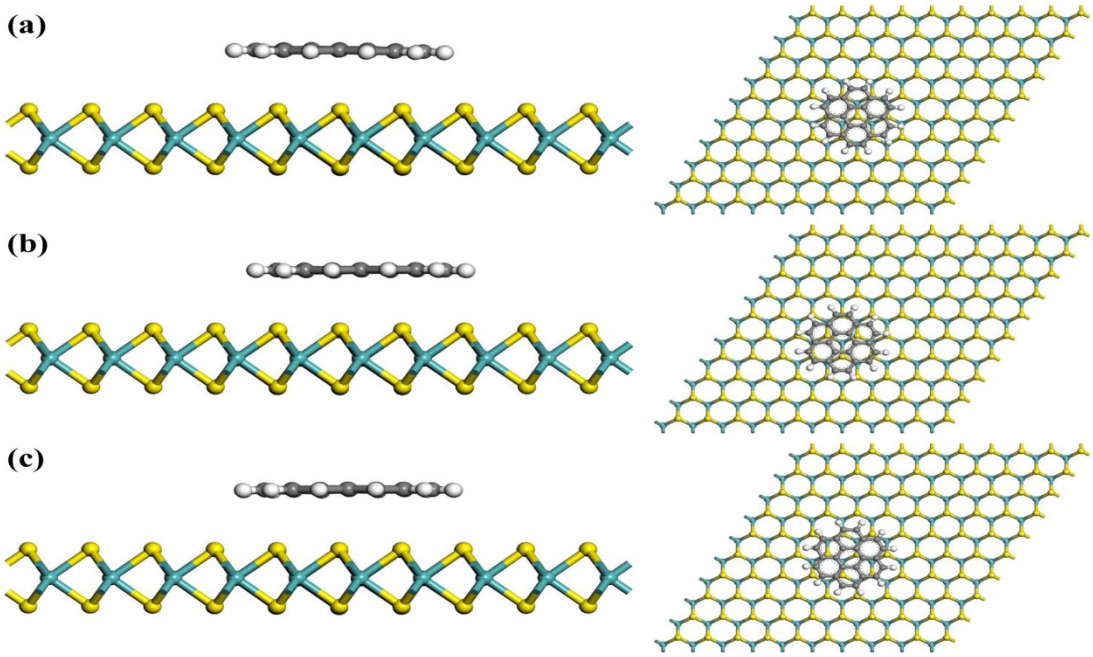

Figure S4 Structures (top view-left and side view-right) of (a) $C_{24}H_{12}$-top, (b) $C_{24}H_{12}$-hollow, and (c) $C_{24}H_{12}$-bridge.

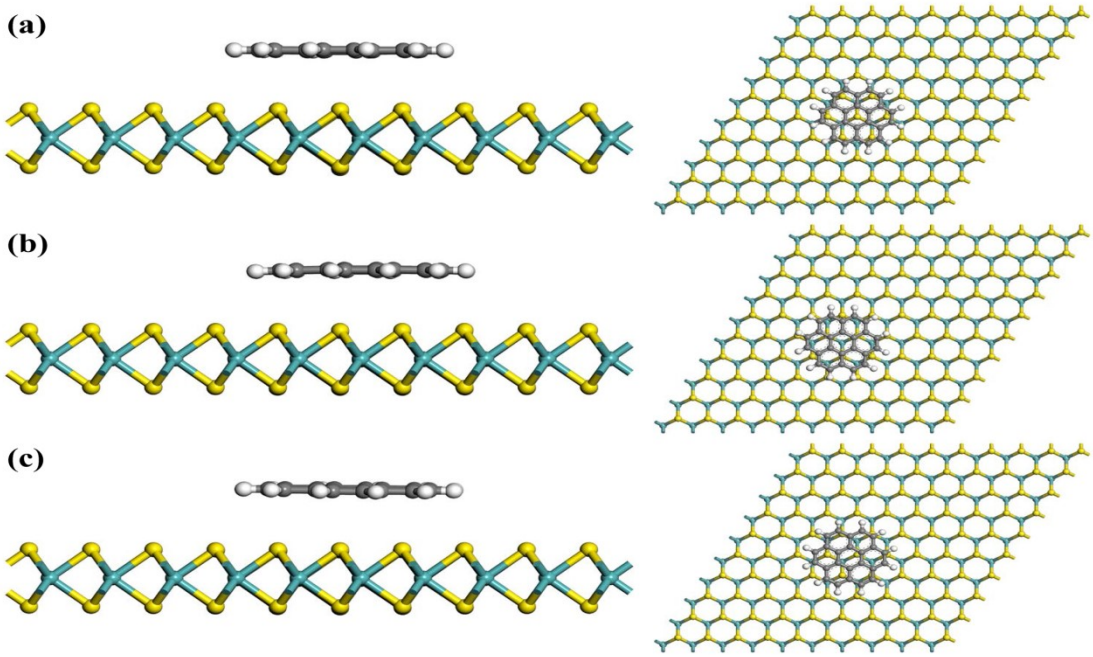

Figure S5 Structures (top view-left and side view-right) of (a) $C_{24}H_{12}$-top30°, (b) $C_{24}H_{12}$-hollow30°, and (c) $C_{24}H_{12}$-bridge30°.

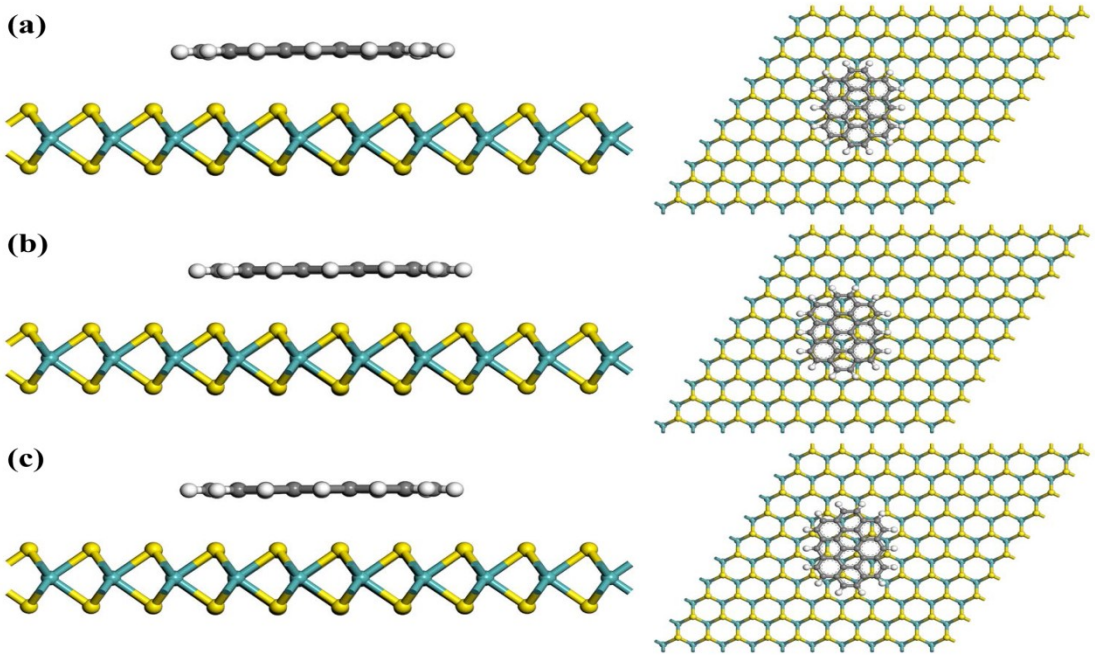

Figure S6 Structures (top view-left and side view-right) of (a) $C_{32}H_{14}$-top, (b) $C_{32}H_{14}$-hollow, and (c) $C_{32}H_{14}$-bridge.

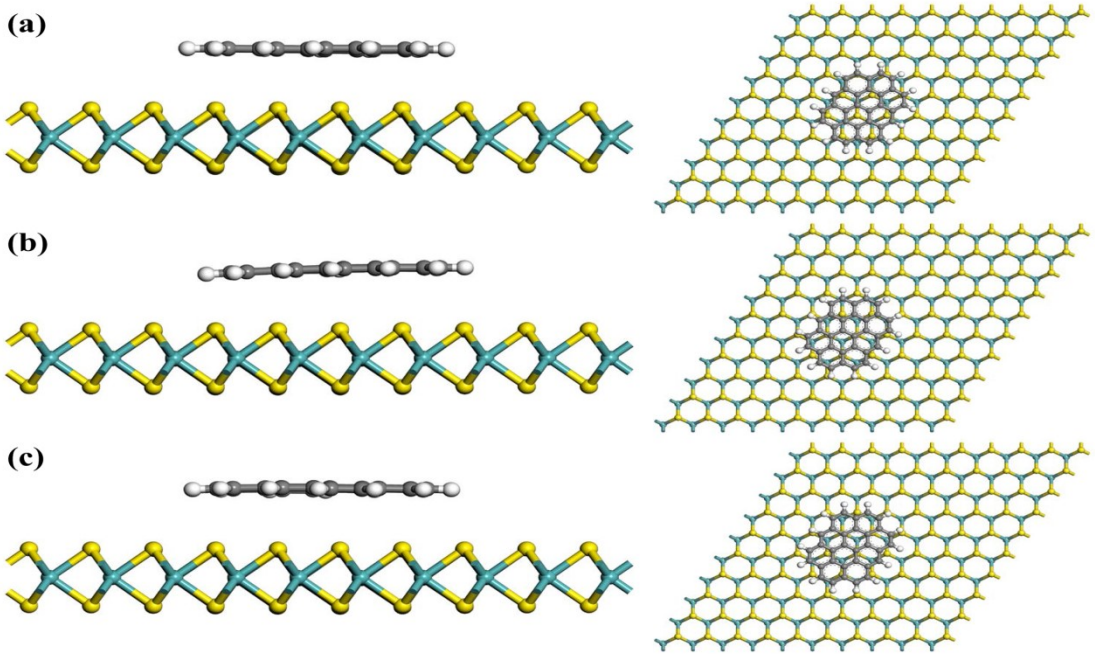

Figure S7 Structures (top view-left and side view-right) of (a) $C_{32}H_{14}$-top30°, (b) $C_{32}H_{14}$-hollow30°, and (c) $C_{32}H_{14}$-bridge30°.

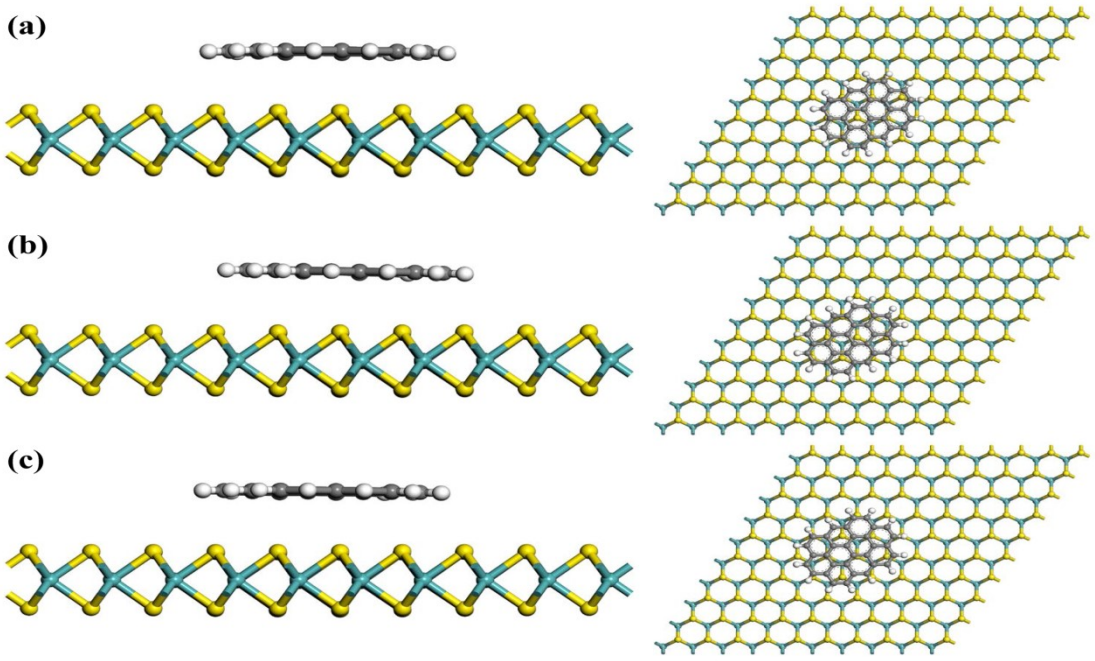

Figure S8 Structures (top view-left and side view-right) of (a) $C_{32}H_{14}$-top60°, (b) $C_{32}H_{14}$-hollow60°, and (c) $C_{32}H_{14}$-bridge60°.

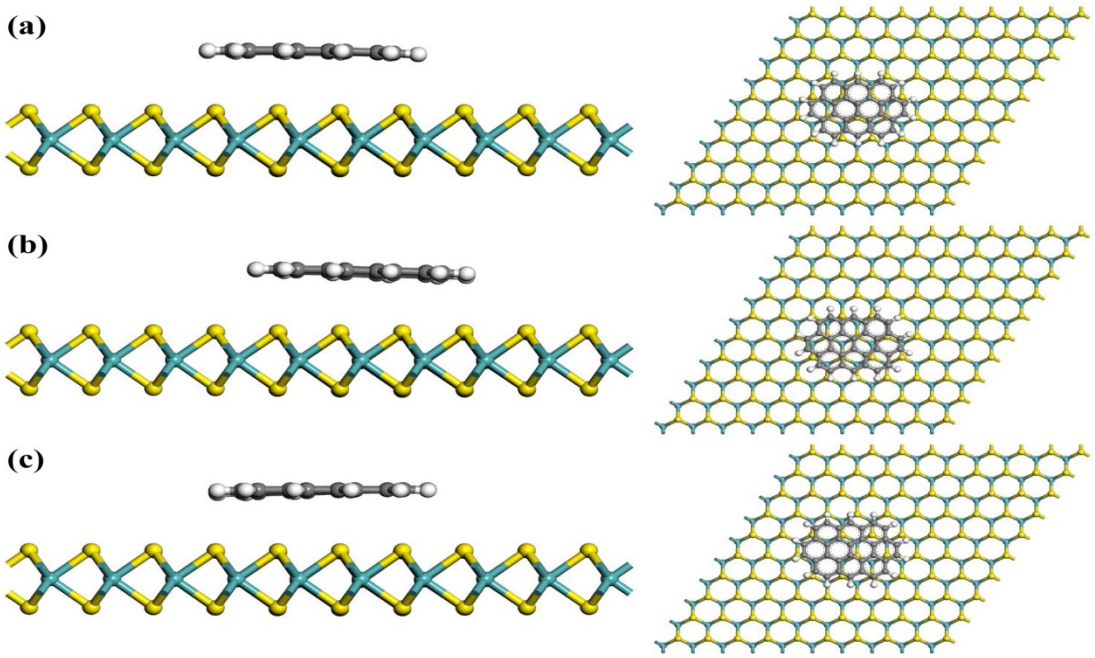

Figure S9 Structures (top view-left and side view-right) of (a) $C_{32}H_{14}$-top90°, (b) $C_{32}H_{14}$-hollow90°, and (c) $C_{32}H_{14}$-bridge90°.

If we further increase the size of GQDs, the interaction between the adjacent GQDs cannot be avoided and the composite is no longer 0D/2D heterojunction. We can infer when the size of GQDs further increase, the conjugate effect of GQDs will be stronger. As the contact area of GQDs and MoS_2 increases, ultimately we can think of it as a 2D/2D graphene-MoS_2 heterojunction. There is much about graphene-MoS_2 research work.[1, 2]

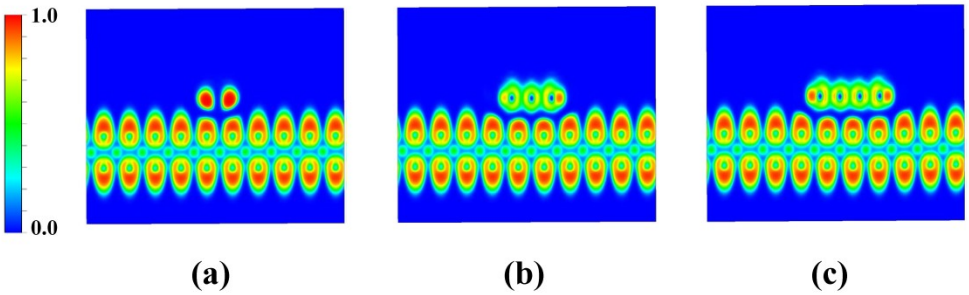

Figure S10 Electron localization function (ELF) of the (a) C_6H_6-MoS_2, (b) $C_{24}H_{12}$-MoS_2 and (c) $C_{32}H_{14}$-MoS_2 along with scaling factor (0–1).

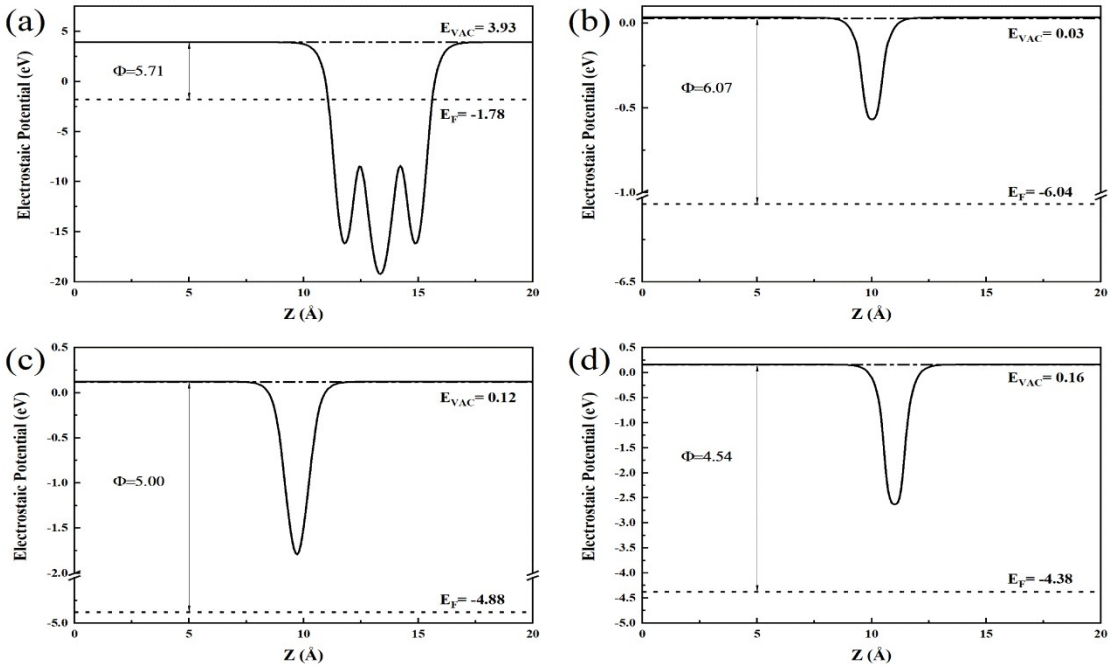

Figure S11 Work function of (a) MoS_2, (b) C_6H_6, (c) $C_{24}H_{12}$, and (d) $C_{32}H_{14}$.

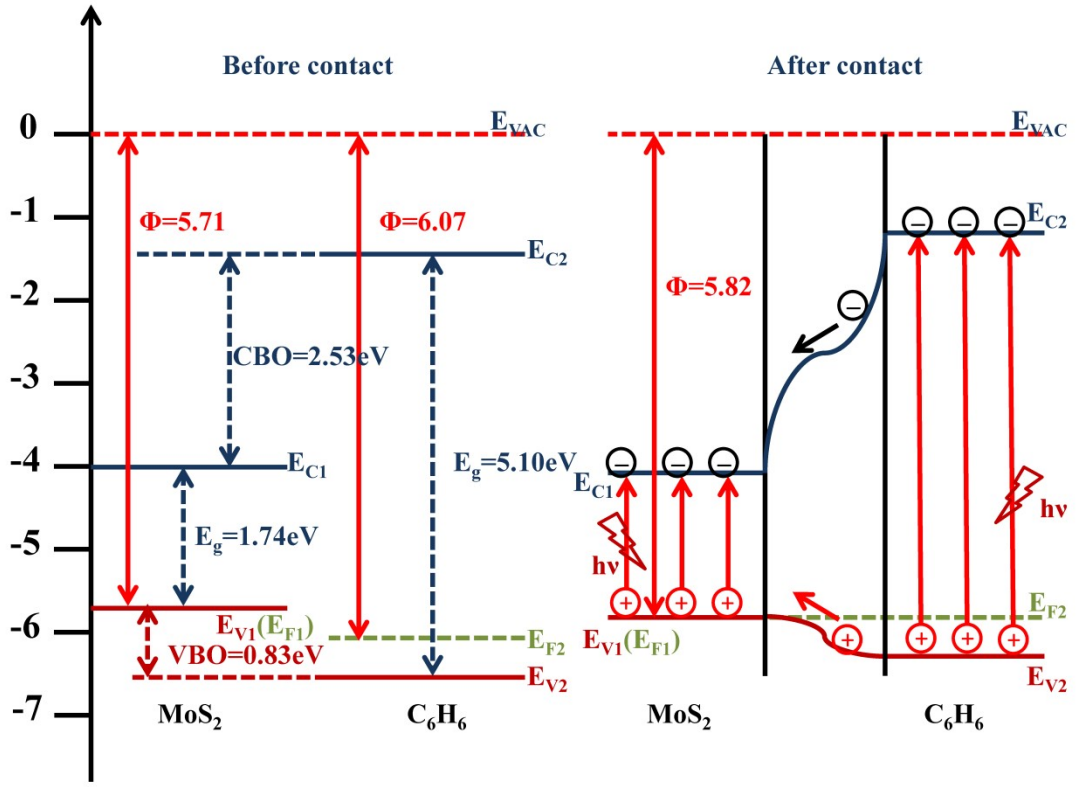

Figure S12 Diagram of the band edge positions before and after contact of MoS_2 and C_6H_6; CBO is the conduction band offset, VBO is the valence band offset, E_{VAC} is the vacuum level, E_C is the bottom of the conduction band, E_V is the top of the valence band, E_g is the band gap, and E_{F1} and E_{F2} are the Fermi levels of MoS_2 and C_6H_6, respectively.

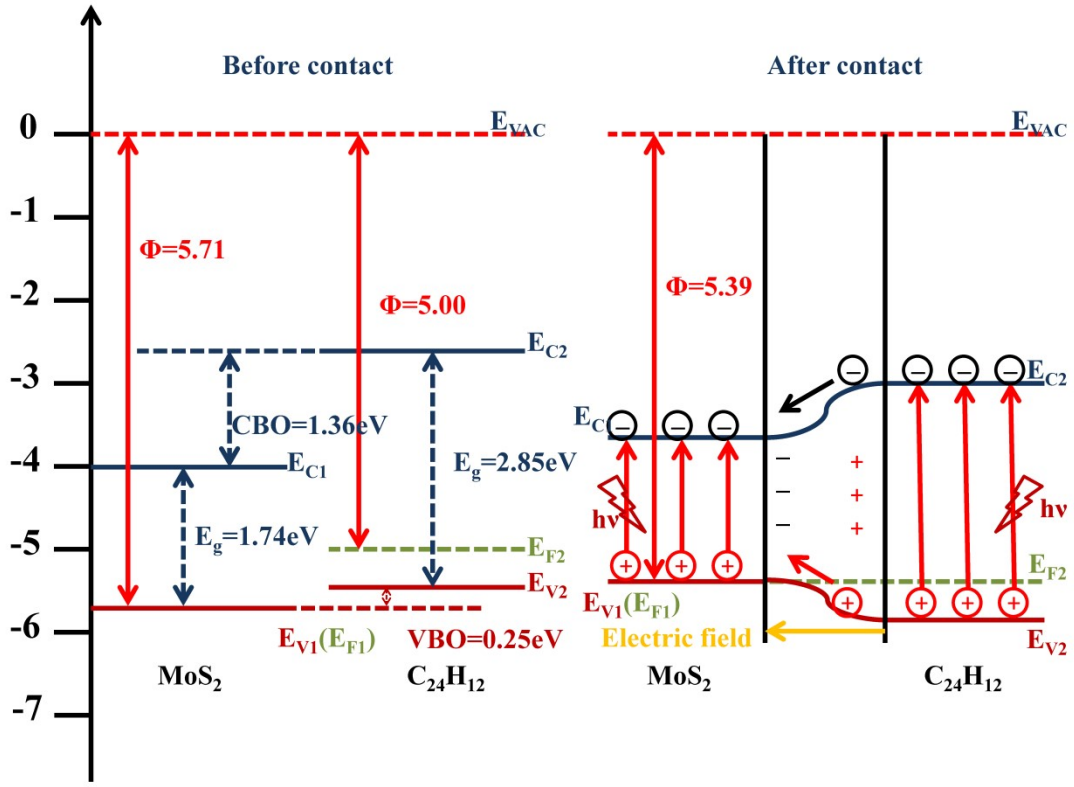

Figure S13 Diagram of the band edge positions before and after contact of MoS_2 and $C_{24}H_{12}$; CBO is the conduction band offset, VBO is the valence band offset, E_{VAC} is the vacuum level, E_C is the bottom of the conduction band, E_V is the top of the valence band, E_g is the band gap, and E_{F1} and E_{F2} are the Fermi levels of MoS_2 and $C_{24}H_{12}$, respectively.

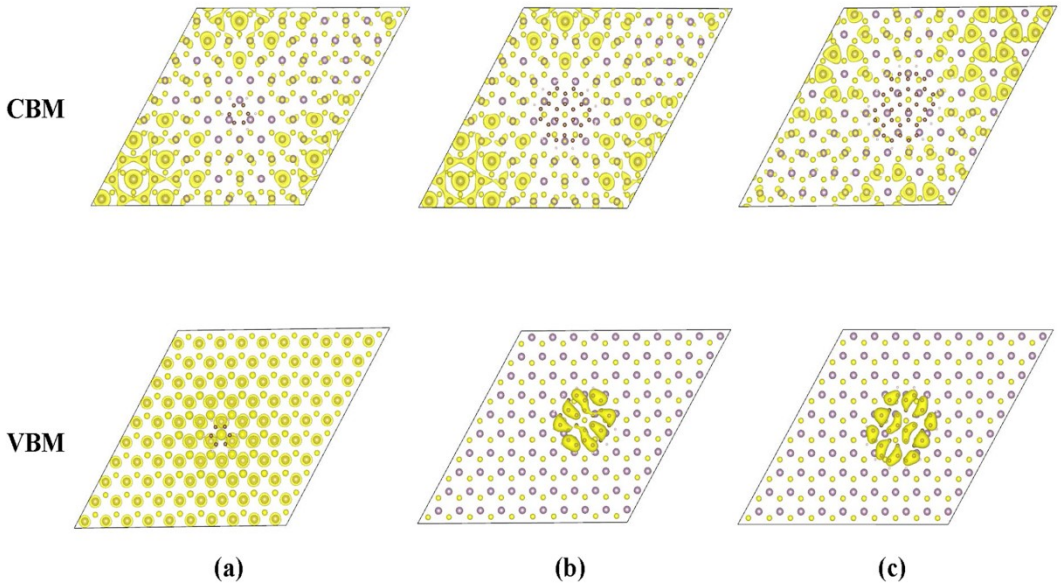

Figure S14 The partial charge densities (top view) of the CBM (upper) and VBM (bottom) for (a) C_6H_6-MoS_2, (b) $C_{24}H_{12}$-MoS_2 and (c) $C_{32}H_{14}$-MoS_2.

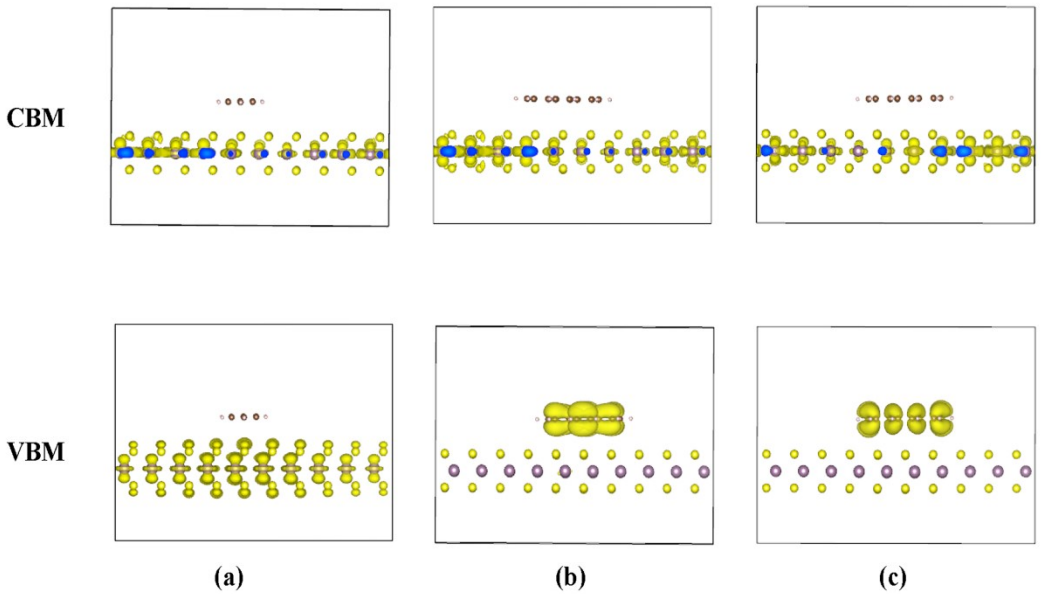

Figure S15 The partial charge densities (side view) of the CBM (upper) and VBM (bottom) for (a) C_6H_6-MoS_2, (b) $C_{24}H_{12}$-MoS_2 and (c) $C_{32}H_{14}$-MoS_2.

As shown in Figure S14-15, the VBMs of $C_{24}H_{12}$-MoS_2 and $C_{32}H_{14}$-MoS_2 are both contributed by GQDs and the CBMs of $C_{24}H_{12}$-MoS_2 and $C_{32}H_{14}$-MoS_2 are both contributed by MoS_2. So their excited state can have charge-transfer (CT) character. As for C_6H_6-MoS_2, the electronic densities of the VBM and the CBM are both primarily localized on MoS_2, which indicate C_6H_6-MoS_2 has locally excited (LE) character.

Table S1 Bnding energy, Binding energy per atom and distance of heterojunctions. A-U represent configurations of S3-S9 from top to bottom orderly.

Configuration	Energy (eV)	Binding energy (eV)	d(Å)
MoS_2	-2234.603		
C_6H_6	-76.107		
$C_{24}H_{12}$	-262.969		
$C_{32}H_{14}$	-343.611		
A	-2311.259	-0.549	3.206
B	-2311.183	-0.473	3.346
C	-2311.229	-0.519	3.273
D	-2499.218	-1.646	3.309
E	-2499.211	-1.639	3.305
F	-2499.215	-1.643	3.304
G	-2499.271	-1.699	3.268
H	-2499.182	-1.610	3.334
I	-2499.238	-1.666	3.309
J	-2580.343	-2.129	3.307
K	-2580.329	-2.115	3.322
L	-2580.345	-2.131	3.325
M	-2580.367	-2.153	3.299
N	-2580.333	-2.119	3.339
O	-2580.321	-2.107	3.340
P	-2580.340	-2.126	3.323
Q	-2580.344	-2.130	3.335
R	-2580.330	-2.116	3.322
S	-2580.340	-2.126	3.329
T	-2580.330	-2.116	3.341
U	-2580.364	-2.150	3.330

Here, “d” is the difference between average positions along the z-axis of S atoms in the upper layer and the centroids of GQDs as shown in Figure S3. Configuration A, G and M are C_6H_6-MoS_2, $C_{24}H_{12}$-MoS_2 and $C_{32}H_{14}$-MoS_2 in the main body, respectively.

Table S2 Bader charge analysis of C_6H_6-MoS_2, $C_{24}H_{12}$-MoS_2 and $C_{32}H_{14}$-MoS_2.

	Charge Transfer (e)	
	MoS_2	**GQDs**
C_6H_6-MoS_2	+0.03	-0.03
$C_{24}H_{12}$-MoS_2	+0.07	-0.07
$C_{32}H_{14}$-MoS_2	+0.08	-0.08

Here, the charge transfer value can be calculated based on the Bader charge[3-6] and it means the amount of charge which MoS_2 or GQDs gained (+) or lost (-) in the process of forming a heterojunction.

Table S3 Work function (eV) of MoS_2, C_6H_6, $C_{24}H_{12}$ and $C_{32}H_{14}$.

	This work	**Calculated values**
MoS_2	5.71	5.88[7]
C_6H_6	6.07	
$C_{24}H_{12}$	5.00	5.29[8]
$C_{32}H_{14}$	4.54	

Table S4. VBM and CBM relative to the absolute vacuum scale (AVS) (eV) before and after contact.

	Before contact		After contact	
	VBM	**CBM**	**VBM**	**CBM**
C_6H_6-MoS_2				
C_6H_6	-6.54	-1.44	-6.29	-1.19
MoS_2	-5.71	-3.97	-5.82	-4.08
$C_{24}H_{12}$-MoS_2				
$C_{24}H_{12}$	-5.46	-2.61	-5.85	-3.00
MoS_2	-5.71	-3.97	-5.39	-3.65
$C_{32}H_{14}$-MoS_2				
$C_{32}H_{14}$	-5.02	-3.07	-5.54	-3.59
MoS_2	-5.71	-3.97	-5.06	-3.32

Table S5. VBM and CBM relative to the normal hydrogen electrode scale (NHE) after contact.

	NHE scale (eV)	
	VBM	**CBM**
C_6H_6-MoS_2		
C_6H_6	1.79	-3.31
MoS_2	1.32	-0.42
$C_{24}H_{12}$-MoS_2		
$C_{24}H_{12}$	1.35	-1.50
MoS_2	0.89	-0.85
$C_{32}H_{14}$-MoS_2		
$C_{32}H_{14}$	1.04	-0.91
MoS_2	0.56	-1.18

1. X. Zheng, J. Xu, K. Yan, H. Wang, Z. Wang and S. Yang, *Chemistry of Materials*, 2014, **26**, 2344-2353.
2. W. Zan, W. Geng, H. Liu and X. Yao, *Journal of Alloys and Compounds*, 2015, **649**, 961-967.
3. Henkelman Group; The University of Texas at Austin, http://theory.cm.utexas.edu/henkelman/research/bader/, Accessed November, 2021.
4. R. F. W. Bader, *Chemical Reviews*, 1991, **91**, 893-928.
5. W. Tang, E. Sanville and G. Henkelman, *Journal of Physics: Condensed Matter*, 2009, **21**, 084204.
6. M. Yu and D. R. Trinkle, *The Journal of chemical physics*, 2011, **134**, 064111.
7. D. Pierucci, H. Henck, J. Avila, A. Balan, C. H. Naylor, G. Patriarche, Y. J. Dappe, M. G. Silly, F. Sirotti, A. T. C. Johnson, M. C. Asensio and A. Ouerghi, *Nano Letters*, 2016, **16**, 4054-4061.
8. L. Cabral, F. P. Sabino, M. P. Lima, G. E. Marques, V. Lopez-Richard and J. L. F. Da Silva, *J. Phys. Chem. C*, 2018, **122**, 18895-18901.